DOI:
10.1242/jcs.235895

Document Version
Peer reviewed version

Rnd3 interacts with TAO kinases and contributes to mitotic cell rounding and spindle positioning

Ritu Garg[1,2], Chuay-Yeng Koo[1], Elvira Infante[2], Caterina Giacomini[1] Anne J. Ridley[2,3] and Jonathan D.H. Morris[1]

[1]King's College London, School of Cancer and Pharmaceutical Sciences, New Hunt's House, Guy's Campus, London SE1 1UL, UK
[2]King's College London, Randall Centre for Cell and Molecular Biophysics, New Hunt's House, Guy's Campus, London SE1 1UL, UK
[3]School of Cellular and Molecular Medicine, University of Bristol, Biomedical Sciences Building, University Walk, Bristol BS8 1TD, UK
Corresponding author: Jonathan D. H. Morris, King's College London, School of Cancer and Pharmaceutical Sciences, New Hunt's House, Guy's Campus, London SE1 1UL; Phone (44)-20-78488302; FAX (44)-20-78486220; E-mail: jonathan.morris@kcl.ac.uk

Keywords: Rnd3, TAOK1, TAOK2, kinase and mitosis

Summary statement: Our results show that TAO kinases bind, phosphorylate and relocate Rnd3 to the cytosol and that Rnd3 can contribute to mitotic cell rounding, spindle positioning and cytokinesis.

ABSTRACT

Rnd3 is an atypical Rho family protein that is constitutively GTP-bound and acts on membranes to induce loss of actin stress fibers and cell rounding. Phosphorylation of Rnd3 promotes 14-3-3 binding and its relocation to the cytosol. Here we show that Rnd3 binds to the thousand-and-one amino acid kinases (TAOK) 1 and 2 *in vitro* and in cells. TAOK1 and TAOK2 can phosphorylate serine residues 210, 218 and 240 near the C-terminus of Rnd3 and induce Rnd3 translocation from the plasma membrane to the cytosol. TAOKs are activated catalytically during mitosis and Rnd3 phosphorylation on serine 210 increases in dividing cells. Rnd3 depletion by RNAi inhibits mitotic cell rounding and spindle centralization and delays breakdown of the intercellular bridge between two daughter cells. Our results show that TAOKs bind, phosphorylate and relocate Rnd3 to the cytosol and that Rnd3 contributes to mitotic cell rounding, spindle positioning and cytokinesis. Rnd3 can therefore participate in the regulation of early and late mitosis and may also act downstream of TAOKs to affect the cytoskeleton.

INTRODUCTION

The sterile 20 (STE20) family of protein kinases includes 28 members, which divide into two groups according to their structure and function (Dan et al., 2001). The six p21-activated kinases (PAKs) have a C-terminal catalytic domain and an N-terminal Cdc42/Rac interacting and binding domain (CRIB), whereas the germinal center kinases (GCKs) possess an N-terminal kinase domain but no CRIB region. PAKs interact with Cdc42 and/or Rac1 via their CRIB domain and act as downstream effectors for these GTPases to regulate the cytoskeleton and cell adhesion however much less is known about the potential interactions between the GCKs and small GTP-binding proteins (Arias-Romero and Chernoff, 2008; Bokoch, 2003; Dan et al., 2001; Delpire, 2009).

The thousand-and-one amino acid kinases (TAOKs, also referred to as prostate-derived STE20-like kinases (PSKs)) belong to the GCK VIII subfamily of STE20 proteins and include TAOK1, TAOK2 and TAOK3 (Chen et al., 1999; Dan et al., 2001; Hutchison et al., 1998; Moore et al., 2000; Zihni et al., 2006). TAOKs regulate microtubule dynamics and organization (Liu et al., 2010; Mitsopoulos et al., 2003; Timm et al., 2003) and also stimulate c-Jun-N-terminal (JNK) and p38 MAPKs (Chen et al., 1999; Hutchison et al., 1998; Moore et al., 2000; Zihni et al., 2006). TAOK1 induces microtubule instability via the phosphorylation of microtubule-associated proteins such as tau, which dissociates from microtubules causing their disassembly (Liu et al., 2010; Tavares et al., 2013; Timm et al., 2003). TAOK2 binds to microtubules directly via its C-terminal region (amino acids 745-1235) and produces stabilized perinuclear microtubules that are resistant to nocodazole-induced depolymerization and contain elevated levels of acetylated α-tubulin (Mitsopoulos et al., 2003). TAOKs are activated catalytically during microtubule-dependent processes, which include mitosis and neuritogenesis (de Anda et al., 2012; Giacomini et al., 2018; Koo et al., 2017; Wojtala et al., 2011). In mitotic cells, phosphorylated and active TAOK1 and TAOK2 localize to the cytoplasm and centrosomes respectively and both proteins are required for mitotic cell rounding and spindle positioning, consistent with their regulatory effects on the cytoskeleton (Koo et al., 2017; Wojtala et al., 2011).

In developing neurons, TAOK2 acts downstream of the Semaphorin 3A receptor neuropilin-1 and regulates axon elongation and basal dendrite formation (de Anda et al., 2012). TAOK2 is phosphorylated by mammalian STE20-like kinase (MST) 3 in neurons and regulates synapse development through enhanced Myosin Va binding and relocation of TAOK2 to the dendrites, where it participates in dendritic spine maturation through stabilization of the post-synaptic density protein 95 (Ultanir et al., 2014; Yadav et al., 2017). TAOK1 can phosphorylate Hippo/MST2 stimulating the Hippo-Salvador-Warts pathway to control tissue growth in Drosophila (Boggiano et al., 2011; Poon et al., 2011).

The Rho family of small GTP binding proteins are well characterized regulators of cytoskeletal and cell adhesion dynamics and control a diverse array of cellular processes including cell morphology, proliferation, migration and division (Jaffe and Hall, 2005). The Rnd proteins 1-3 are atypical Rho GTP-binding proteins due to their lack of intrinsic GTPase activity and are constitutively GTP-bound (Chardin, 2006; Riou et al., 2010). Like most other Rho family members, Rnd proteins are post-translationally prenylated at the C-terminus, enabling them to associate with membranes (Seabra, 1998). Rnd3 (also referred to as RhoE) behaves antagonistically to RhoA and functions to increase p190RhoGAP activity towards RhoA and induces loss of integrin-mediated focal adhesions leading to disassembly of actin stress fibers and cell rounding (Guasch et al., 1998; Nobes et al., 1998; Wennerberg et al., 2003).

Rnd3 also binds to and is a substrate of Rho-associated coiled coil kinase 1 (ROCK1), which functions to inhibit Rnd3 (Komander et al., 2008; Riento et al., 2003). In addition, Rnd3 associates with RhoGEF Syx and plexin-B2 and can induce thin cellular protrusions and cell rounding respectively (Goh and Manser, 2012; McColl et al., 2016; Wennerberg et al., 2003). Rnd3 therefore regulates a diverse array of processes including neuronal polarity, cell cycle progression, phagocytosis, cell migration and embryonic development in different cell types but potential roles for Rnd3 during mitosis have not been investigated (Azzarelli et al., 2015; Chardin, 2006; Riento et al., 2005b).

The inability of Rnd proteins to hydrolyze GTP has led to the identification of alternative mechanisms to regulate their activity including alterations in protein expression and stability, and through post-translational modifications such as phosphorylation (Hodge and Ridley, 2016; Riento et al., 2005a; Riento et al., 2005b; Riou et al., 2013; Riou et al., 2010). Critically, the phosphorylation of C-terminal residues on Rnd3 by ROCK1 and Protein Kinase C (PKC) enhances 14-3-3 binding to relocate Rnd3 from its active site on membranes to the cytosol (Madigan et al., 2009; Riento et al., 2005a; Riou et al., 2013). Rnd3 phosphorylation also reduces its ability to interact with p190RhoGAP (Komander et al., 2008; Riou et al., 2013).

In this study, a new role for Rnd3 in mitotic cell rounding, spindle centralization and cytokinesis is demonstrated and we show that TAOK1 and TAOK2 can bind, phosphorylate and relocate Rnd3 from the plasma membrane to the cytosol. Rnd3 therefore regulates cell morphology and spindle positioning during mitosis and is a novel TAOK substrate.

RESULTS

Rnd3 binds to TAOK1 and TAOK2

Previous studies have shown that TAOKs are activated during mitosis and contribute to mitotic cell rounding whereas overexpressed Rnd3 induces a “rounded” morphology in interphase cells (Guasch et al., 1998; Nobes et al., 1998; Wojtala et al., 2011). Given this similarity in phenotype we investigated whether TAOK1 or TAOK2 interacted with Rnd3. We found that TAOK1 and TAOK2 coimmunoprecipitated with Rnd3 (Fig. 1A,B). In addition, TAOK1 and TAOK2 expressed in COS-7 cells associated with GST-Rnd3 (Fig. 1C) and purified GST-TAOK1 (1-314) and GST-TAOK2 (1-314) pulled down recombinant His-Rnd3 (Fig. 1D) suggesting that these proteins interact directly. We have shown previously that TAOK2 is expressed as a protein doublet (165 and 185 kDa) (Moore et al., 2000) and interestingly Rnd3 appears to bind preferentially to the 185-kDa form of TAOK2. Kinase-defective TAOK1 (K57A) and TAOK2 (K57A) bound to Rnd3 *in vitro* and in cells demonstrating that TAOK catalytic activity is not required for Rnd3 association (Fig. 1A,B). Taken together, these results show that TAOK1 and TAOK2 can associate with Rnd3 independently of TAOK catalytic activity.

Rnd3 is phosphorylated by TAOKs

We have shown previously that a TAOK-pS181 antibody detects catalytically active forms of TAOK1 and TAOK2, which are phosphorylated on serine residue 181 as part of their conformational activation (Koo et al., 2017; Wojtala et al., 2011; Zhou et al., 2004; Zihni et al., 2007). Active TAOK-pS181 increases during mitosis (Koo et al., 2017; Wojtala et al., 2011). To determine whether Rnd3 can stimulate TAOK catalytic activity, NIH3T3 fibroblasts expressing Rnd3 in a tetracycline (Tet) on/Tet off-inducible system were used (Villalonga et al., 2004). Exogenous Rnd3 induced cell rounding and branched protrusions in these cells (Fig. S1A,B), as reported previously, but did not increase TAOK activity in interphase or mitotic cells (Fig. 2A) (Villalonga et al., 2004). In contrast, enhanced TAOK-pS181 staining was detected in mitotic cells incubated with or without Tet consistent with our previous observations (Fig. 2A) (Koo et al., 2017; Wojtala et al., 2011). These results show that Rnd3 overexpression is not sufficient to enhance TAOK activity.

We then investigated whether Rnd3 is a substrate for TAOKs. We focused on three serine residues 210 (S210), 218 (S218) and 240 (S240) located in the C terminus of Rnd3 because these sites have been shown to regulate Rnd3 localization and function (Riou et al., 2013). We used plasmids encoding mutated Rnd3 proteins, which included a construct where all seven known Ser/Thr sites were replaced by alanine (AllA-Rnd3) or where single residues had been restored to produce AllA-S210, AllA-S218 or AllA-S240 Rnd3 (Riou et al., 2013). Catalytically active recombinant TAOK1 and TAOK2 phosphorylated wild type (WT) Rnd3 but not AllA-Rnd3 (Fig. 2B).

Analysis of individual Rnd3 sites show that AllA-S210, AllA-S218 and AllA-S240 are all phosphorylated by TAOK1 and TAOK2 (Fig. 2B). Purified TAOK1 or TAOK2 were also incubated with recombinant Rnd3 for *in vitro* kinase assays and both kinases increased Rnd3-pS210 phosphorylation (Fig. 2C). These results show that TAOKs can phosphorylate Rnd3 on three serine residues involved in regulating Rnd3 localization and function (Riou et al., 2013; Riou et al., 2010).

TAOKs relocate Rnd3 from the plasma membrane to the cytosol

Previous studies have shown that ROCK1 phosphorylates and translocates Rnd3 from the plasma membrane to the cytosol, where it is inactive (Riento et al., 2005a; Riou et al., 2013). The phosphorylation of Rnd3 on S210, S218 and S240 by TAOK1 and TAOK2 suggests that these kinases may also alter Rnd3 localization and function. To address this possibility, the effect of TAOKs on Rnd3 localization was analyzed biochemically. In control cells, Rnd3 was distributed equally between the membrane and cytosolic fractions (Fig. 3A,B). In contrast, coexpression of Rnd3 with TAOK1, TAOK2 or ROCK1 (1-420) increased the proportion of Rnd3 in the cytosol and reduced the amount of Rnd3 in the membrane fraction, suggesting that Rnd3 is likely to be phosphorylated and translocated to the cytosol (Fig. 3A,C). Kinase-defective TAOK1 (K57A) and TAOK2 (K57A) did not increase the proportion of Rnd3 in the cytosol compared to the membrane as effectively as wild type TAOKs demonstrating a requirement for the catalytic activity of these proteins (Fig. 3B,C). In addition, TAOK1 and TAOK2 did not increase cytosolic AllA-Rnd3 significantly (Fig. 3D). In some experiments Rnd3 was detected in the nuclear fraction, which may contain the endoplasmic reticulum where Rho/CAAX proteins are processed (Manolaridis et al., 2013; Michaelson et al., 2001). The transmembrane protein N-Cadherin remained in the membrane fraction and GAPDH was detected in the cytosol under all conditions (Fig. 3A,B).

The effects of TAOKs on Rnd3 localization was also examined by immunofluorescence. MCF-7 breast cancer cells were used because they form tight colonies in which each individual cell maintains close contacts with its neighboring cells to provide a defined membrane. In MCF-7 cells expressing Rnd3 alone, Rnd3 localized at the plasma membrane and at cell-cell contacts (Fig. 3E,F). Rnd3 was translocated to the cytosol in the presence of catalytically active TAOK1 or TAOK2 but not with kinase-defective TAOK1 (K57A) or TAOK2 (K57A) (Fig. 3E,F). These results are consistent with our cell fractionation studies showing that TAOK1 and TAOK2 are able to relocate Rnd3 from the membrane to the cytosol in cells.

Rnd3 depletion inhibits mitotic cell rounding and spindle centralization

TAOKs are active and may therefore target Rnd3 during mitosis (Koo et al., 2017). To better understand Rnd3 function in dividing cells, HeLa cells were transfected with small interfering RNAs (siRNAs) targeting Rnd3. Control mitotic cells have a rounded morphology and a centralized spindle, which is characteristic of dividing HeLa cells (Fig. 4A-C). Rnd3 depletion inhibited mitotic cell rounding and produced irregularly shaped cells that contained a decentralized spindle located to one side of the dividing cell (Fig. 4A-C). Rnd3 depletion also increased the spread area of mitotic cells and produced a more flattened and elongated cell morphology (Fig. 4A,D). Rnd3 depletion was confirmed by immunoblotting (Fig. 4E,F; Fig. S2). These results demonstrate that Rnd3 can contribute to mitotic cell rounding and spindle positioning during cell division.

Rnd3 depletion delays cytokinesis

We next examined the effect of depleting Rnd3 on the duration of mitosis using a HeLa cell line stably expressing mCherry-α-tubulin. Analysis of cells using time-lapse microscopy showed that the time taken for mitotic cells to complete cytokinesis (intercellular bridge formation to abscission) increased in Rnd3-depleted cells when compared to control cells (Fig. 5A). In particular, movies and stills produced using time-lapse microscopy revealed that silencing Rnd3 delayed breakdown of the intercellular bridge between two daughter cells and this structure was retained and intact 180 min after nuclear envelope breakdown (Fig. 5A,B and Movies S1-3 showing representative cells). No intercellular bridges were observed in control cells at this time point (Fig. 5A). These results indicate that Rnd3 expression is required for cells to complete cytokinesis in the normal time frame and to facilitate breakdown of the intercellular bridge and separation of daughter cells.

Rnd3 and TAOKs have opposing effects on spindle polarity

A previous study using mitotic cells with supernumerary centrosomes reported that a reduction in actomyosin contractility via the discoidin domain receptor 1 (DDR1) and Rnd3 prevents efficient centrosome clustering (Rhys et al., 2018). Here, we found that the TAOK inhibitor compound 43 (Cpd 43) (Koo et al., 2017) induced centrosome amplification and multipolar spindles in mitotic cells and that Rnd3 depletion was unable to reverse this phenotype (Fig. S3A,C). Depletion of Rnd3 did however reduce the percentages of mitotic cells exhibiting multipolar spindles following cell treatment with the actin depolymerizing agent Dihydrocytochalasin B (DCB) (Fig. S3B,C) as reported previously (Rhys et al., 2018). Rnd3 depletion was confirmed by immunoblotting (Fig. S3D,E). TAOK activity therefore prevents centrosome amplification and maintains spindle bipolarity but this process occurs independently of Rnd3.

Rnd3 is phosphorylated in mitotic cells

Active TAOK-pS181 increases during mitosis and is present in the cytoplasm and at the spindle poles in dividing cells (Fig. 6A) (Koo et al., 2017). Here, we used a phospho-Rnd3 antibody that recognizes Rnd3 phosphorylated on S210 (Rnd3-pS210) (Fig. S1C,D) and labeled mitotic cells specifically (Fig. 6B), and was similar to the TAOK-pS181 antibody. Rnd3-pS210 localized to the cytosol and punctate sites (Fig. 6B). In control experiments, pretreatment of the Rnd3-pS210 antibody with the phosphorylated Rnd3-pS210 peptide, but not the nonphosphorylated Rnd3-S210 peptide, significantly reduced the Rnd3-pS210 antibody staining in mitotic cells (Fig. 6B). Nocodazole was used to increase the number of mitotic cells and TAOK-pS181, Rnd3-pS210 and Histone H3-pS10 were detected in cell lysates (Fig. 6C). In contrast, the phosphorylation of these proteins decreased 4 h after nocodazole removal when cells are likely to exit mitosis and re-enter the cell cycle, as we have shown previously (Wojtala et al., 2011). Active TAOK-pS181 and phosphorylated Rnd3-pS210 are therefore present in mitotic cells, consistent with a potential role for TAOKs in phosphorylating Rnd3 during cell division.

DISCUSSION

TAOKs regulate the microtubule cytoskeleton and mitosis but whether this involves interactions with small GTP-binding proteins has not previously been investigated (Chen et al., 1999; Hutchison et al., 1998; Liu et al., 2010; Mitsopoulos et al., 2003; Moore et al., 2000; Zihni et al., 2006). Here, we identify Rnd3 as a new binding partner for TAOK1 and TAOK2. Rnd3 does not increase TAOK catalytic activity but is a good substrate for TAOK1 and TAOK2 which phosphorylate Rnd3 on three C-terminal residues, S210, S218 and S240 and relocate Rnd3 away from the plasma membrane to the cytosol. Mutational analysis has shown previously that the phosphorylation of Rnd3 on S240 is essential, and additional phosphorylation on S210 or S218 required, for optimal 14-3-3 binding and cytosolic localization of Rnd3 (Riou et al., 2013). We show that Rnd3 phosphorylation on S210 increases during mitosis when TAOKs are active and Rnd3-pS210 localizes to the cytosol but was not detected on the plasma membrane. The Rnd3-pS210 antibody also produced punctate staining in mitotic cells. Previous studies have shown that Rnd3 localizes on the trans-Golgi network however further investigations are needed to determine where Rnd3-pS210 localizes (Riento et al., 2003). We have also demonstrated that Rnd3 depletion delays cytokinesis and alters mitotic cell shape, identifying a new function for Rnd3 in mitosis.

The onset of mitosis is commonly accompanied by cell rounding, which involves the disassembly of focal adhesions, reduced cell attachment and the assembly of a dense actin cortex at the plasma membrane (Kunda and Baum, 2009; Lancaster and Baum, 2014; Rosenblatt et al., 2004). The rounded cell morphology locates the centrosomes and spindle in close proximity to the actin cortex, which in turn facilitates spindle assembly and positioning (Heng and Koh, 2010; Kunda and

Baum, 2009). We have shown previously that TAOKs contribute to mitotic cell rounding and spindle positioning (Wojtala et al., 2011). Consistent with a mechanistic link between TAOKs and Rnd3, we report here that Rnd3 depletion inhibits mitotic cell rounding and produces irregularly shaped cells containing a decentralized spindle. Spindle orientation and positioning requires contact between the astral microtubules and cortex to exert pushing forces on the spindle poles as well as cortical pulling forces (Grill and Hyman, 2005; Pearson and Bloom, 2004). Our data suggest that the disruption of cell rounding by Rnd3 silencing may interfere with the actin cortex and generation of forces needed to position the spindle centrally. In addition, Rnd3 can antagonize RhoA through its interaction with p190RhoGAP and these proteins may cooperate to regulate the actin cytoskeleton during cell division (Wennerberg et al., 2003). RhoA activity promotes mitotic cell rounding and cortical stiffening at the beginning of mitosis whereas Rnd3 has the opposite effect, presumably through its ability to antagonize RhoA-induced actomyosin contractility (Hidalgo-Carcedo et al., 2011; Maddox and Burridge, 2003; Riento et al., 2003).

We found that the duration of mitosis increases in Rnd3 depleted cells and observed a delay in breakdown of the intercellular bridge between daughter cells at the end of cytokinesis. RhoA activity peaks during anaphase-telophase stimulating formation of the actomyosin contractile ring and ingression of the cleavage furrow (Chircop, 2014; Derksen and van de Ven, 2017; Piekny et al., 2005; Piekny and Glotzer, 2008; Thery and Bornens, 2006). Moreover, RhoGEF Ect2 localizes to the spindle midzone stimulating RhoA during early cytokinesis whereas RhoGEF-H1 enhances RhoA activity towards the end of cytokinesis (Birkenfeld et al., 2007). Notably, the RhoA GAP protein p190RhoGAP is detected at the cleavage furrow and RhoA activity must be downregulated during furrow ingression to avoid cytokinetic defects (Manchinelly et al., 2010; Su et al., 2003). Depletion of p190RhoGAP enhances RhoA activity in the furrow and results in failure of the cytokinetic furrow to progress to abscission (Manukyan et al., 2015). p190RhoGAP is required to regulate furrow ingression and Rnd3 depletion may therefore increase RhoA activity by reducing p190RhoGAP activity and thereby delay cytokinesis in the same way as depleting p190RhoGAP (Manukyan et al., 2015). RhoA inactivation also occurs during the final stages of abscission, when the actomyosin contractile ring is dismantled and cortical actin depolymerized within the intercellular bridge, which most likely involves enhanced RhoGAP activity (Chircop, 2014). We found that Rnd3 depletion delays breakdown of the intercellular bridge between daughter cells demonstrating a requirement for Rnd3 towards the end of mitosis. Mechanistically, the midbody between daughter cells is stabilized by a septin-anillin complex during late cytokinesis and the ESCRTIII protein complex recruited to the abscission site to complete abscission (Addi et al., 2018). It is possible that Rnd3 also affects these steps of cytokinesis, in addition to its other roles in mitosis.

Rnd3 can therefore contribute to cell rounding and spindle positioning during early mitosis and cytokinesis towards the end of mitosis. Its effects on mitosis are consistent with inhibiting RhoA activity. Other examples of Rnd3 acting antagonistically to RhoA include membrane blebbing (Aoki et al., 2016). In expanding blebs, Rnd3 and p190RhoGAP localize to the membrane lacking cortical actin and inhibit RhoA and ROCK. In contrast, RhoA and ROCK are recruited to the membrane at the start of bleb retraction and their activity and actomyosin contractility increases (Aoki et al., 2016). Furthermore, ROCK1 phosphorylates and relocates Rnd3 away from the membrane to the cytosol (Aoki et al., 2016). In another study, actomyosin contractility is reduced by E-cadherin/DDR1/Rnd3 in cells containing supernumerary centrosomes resulting in multipolar spindles (Rhys et al., 2018). We found that inhibition of TAOK activity alone stimulates centrosome amplification and multipolar division but we were unable to rescue this phenotype by silencing Rnd3. This implies that TAOKs do not act through Rnd3 to prevent multipolar spindle formation and this TAOK function presumably involves other TAOK substrates. One possibility is septin 7, which is a known TAOK substrate: septins are known to be involved in regulating cleavage furrow contraction and cytokinetic bridge stability (Addi et al., 2018; Estey et al., 2010).

In conclusion, we have shown that TAOKs bind, phosphorylate and relocate Rnd3 to the cytosol and that Rnd3 can contribute to mitotic cell rounding, spindle positioning and cytokinesis. Our results identify new roles for Rnd3 in regulating early and late mitosis and suggest that Rnd3 acts downstream of TAOKs to contribute to the effects of these kinases on the cytoskeleton during mitosis.

MATERIALS AND METHODS

Plasmids and Reagents

pRK5-Myc-TAOK1, pRK5-Myc-TAOK1 (K57A), pRK5-Myc-TAOK2, pRK5-Myc-TAOK2 (K57A), pGEX-GST-Rnd3, p-EGFP, p-EGFP-Rnd3 and CMV-FLAG-Rnd3 (wild type (WT), AllA, AllAS210, AllAS218 or AllAS240) were described previously (Moore et al., 2000; Riento et al., 2005a; Riou et al., 2013; Zihni et al., 2006). TAOKs were subcloned into the N-GFP-CB6 vector kindly provided by Professor Way (Francis Crick Institute, UK). pCAG-Myc-ROCK1 was obtained from Professor Narumiya (Kyoto, Japan). Recombinant glutathione-S-transferase (GST)-TAOK1 (1-314) and GST-TAOK2 (1-314) proteins were purchased from SignalChem (T24-11G and T25-11G) and recombinant His-Rnd3 was obtained from Abcam (ab97952). Glutathione-sepharose beads 4B were purchased from GE Healthcare (17-0756-01). Protein A agarose beads were obtained from ThermoFisher Scientific (15918-04). SiRNAs were obtained from Dharmacon or Merck (Sigma-Aldrich) and had the following sequences, nontargeting siControl (UAGCGACUAAACACAUCAA), siRnd3-7 (UAGUAGAGCUCUCCAAUCA) and siRnd3-9 (GCGGACAGAUGUUAGUACA) (McColl et al., 2016). Rnd3-pS210 phosphorylated peptide (H_2N-CKNVKRNKS (PO_3H_2) QRA-$CONH_2$) and

the nonphosphorylated Rnd3-S210 peptide (H_2N-CKNVKRNKSQRA-$CONH_2$) were supplied by Eurogentec. Dihydrocytochalasin B (DCB) (D1641), 4′, 6-Diamidino-2-phenylindole dihydrochloride (DAPI) (D9542), thymidine (T9250), nocodazole (M1404) and goat serum (G9023) were purchased from Merck (Sigma-Aldrich). TAOK inhibitor compound 43 (Cpd 43) was synthesized by Evotec Limited (UK) (Koo et al., 2017). 4% paraformaldehyde (PFA)/phosphate buffered saline (PBS) was purchased from AlfaAesar.

Antibodies

Affinity-purified TAOK-pS181 (1:1000) and Rnd3-pS210 (1:250) rabbit antibodies were described previously (Riou et al., 2013; Zihni et al., 2007). Antibodies were obtained from the following sources: rabbit anti-TAOK1 (1:1000, 26250) and anti-TAOK2 (1:1000, 21188) (Proteintech); rabbit anti-Histone H3-pS10 (1:1000, 06-670), mouse anti-Rnd3 (1:500, 05-725) and mouse anti-GAPDH (1:10000, MAB374) antibodies (Merck Millipore); rabbit polyclonal anti-FLAG (1:1000, clone M2) (F-7425), mouse anti-FLAG agarose beads (A2220), mouse anti-α-tubulin (1:1000, T9026, clone DM1A), mouse anti-Myc antibody (1:1000, 13-2500, clone 9E10), rabbit anti-GFP antibody (1:1000, A-11122) and mouse anti-HA antibody bound to agarose (clone HA.7) (A2095) (Merck, Sigma-Aldrich); rabbit anti-pericentrin (1:500, ab4448, Abcam) and mouse anti-HA antibody (1:1000, MMS-101R, BioLegend (Covance)); rabbit polyclonal anti-N-Cadherin (1:1000, H-13116) (Cell Signaling Technology) and rat monoclonal anti-HA antibody (1:1000, 11867 423001, clone 3F10) (Roche); rabbit polyclonal anti-MAD2 (1:500, A300-301A) (Bethyl Laboratories); rabbit polyclonal anti-ERK1 (1:1000, sc-94) and mouse monoclonal anti-GST (B14) (1:1000, sc-138) and anti-ROCK1 (G6) (1:500, sc-17794) antibodies (Santa Cruz Biotechnology). Secondary antibodies were horse-radish peroxidase (HRP)-linked polyclonal goat anti-mouse IgG (1:2000, P0447) and goat anti-rabbit IgG (P0448) or rabbit anti-goat IgG (1:2000, P0449) (Agilent); goat anti-rat IgG (1:2000, sc-2006) (Santa Cruz Biotechnology); goat anti-rabbit Alexa-Fluor 568 (1:200, A11036) or goat-anti-rabbit Alexa-Fluor 546 (1:400, A11010), goat anti-mouse Alexa-Fluor 546 (1:400, A11003), goat anti-mouse Alexa-Fluor 488 (1:400, A11029) or Alexa-Fluor 633 Phalloidin (1:200, A22284) (ThermoFisher Scientific).

Cell culture and transfection

COS-7 (obtained from Michael Waterfield, Ludwig Institute for Cancer Research), HeLa (obtained from Jeremy Carlton, Francis Crick Institute, London; authenticated 2016) or HaCaT (obtained from Susana Godinho, Bart's Cancer Institute-Queen Mary University of London) (Rhys et al., 2018) cells were grown in Dulbecco's modified Eagle's medium (DMEM) containing 10% fetal calf serum (FCS) (ThermoFisher Scientific). MCF-7 breast cancer cells (obtained from ATCC; authenticated 2016) were cultured in McCoy's/5A medium supplemented with 10% FCS (ThermoFisher Scientific). NIH3T3-Rnd3 inducible fibroblasts (Villalonga et al., 2004) were grown in DMEM supplemented with 10% donor calf serum and treated with 0.5 µg/ml tetracycline (Tet)

and puromycin. Media was checked routinely for mycoplasma using DAPI staining. For electroporation, COS-7 cells were washed with ice-cold PBS, detached using trypsin and centrifuged. The cell pellet was resuspended in 250 µl of cold electroporation buffer (120 mM KCl, 2 mM $MgCl_2$, 0.5% Ficoll, 25 mM HEPES and 10 mM K_2PO_4/KH_2PO_4 pH 7.6) and samples electroporated at 250 V and 960 µF with 5 µg of DNA using a BioRad GenePulser. The cells were plated on 10 cm^2 dishes and incubated for 24 h prior to lysis. For transient transfection, HeLa, MCF-7 or HaCaT cells were treated with the indicated plasmids and Lipofectamine 2000 used according to the manufacturer's instructions (ThermoFisher Scientific) (Wojtala et al., 2011). For Rnd3 depletion experiments, HeLa or HaCaT cells were plated on glass coverslips (or 6-well dishes or Ibidi live cell imaging plates) and transfected with the indicated siRNA oligonucleotides (50 nM) using Oligofectamine in Optimem (ThermoFisher Scientific). After 6 h, Optimem was removed and replaced with DMEM containing 10% FCS (growth medium) and cultures incubated for 72 h unless stated otherwise. For drug treatment with DCB (4 µM), HaCaT cells were transfected with the indicated siRNAs for 6 h, Optimum removed and replaced with growth medium containing DCB for 20 h and cells then incubated in growth medium for a further 24 h before fixation (Rhys et al., 2018). Alternatively, siRNA transfected HaCaT cells were incubated in growth medium for 48 h and treated with Compound 43 (10 µM) for a further 24 h before fixation. For expression of HA-Rnd3 in NIH3T3-Rnd3 fibroblasts containing a Tet-off inducible HA-Rnd3 construct (pTRE-HA-Rnd3), cultures were incubated in the absence of Tet for 8 h (Villalonga et al., 2004).

Immunoprecipitations and GST pulldowns

COS-7 cells were lysed using ice-cold cell lysis buffer (130 mM NaCl, 1% Triton X-100, 1 mM dithiothreitol, 10 mM NaF, 0.1 mM Na_3VO_4, 1 mM phenylmethylsulfonyl fluoride, 1% aprotinin, 10 µg/ml leupeptin and 20 mM Tris-HCl pH 8.0). After centrifugation (16g / 10 min/4ºC), the supernatants were incubated with 20 µl of green fluorescent protein (GFP)-Trap beads (Chromotek) for 2 h at 4ºC with rotation. The beads were washed extensively with lysis buffer and bound proteins analyzed by SDS-PAGE and immunoblotting. For pulldown assays, recombinant GST (control) or GST-Rnd3 fusion proteins were expressed in *E. coli* and purified as described previously (McColl et al., 2016). Electroporated COS-7 cells were washed and extracted in lysis buffer. Cell lysates were combined with 10 µg recombinant GST or GST-Rnd3 bound to glutathione-sepharose beads for 2 h at 4°C and beads washed extensively with lysis buffer. Alternatively, recombinant His-Rnd3 (0.3 µg) was incubated with 0.3 µg GST-tagged TAOK1 (1-314) or TAOK2 (1-314) (2 h / 4°C) followed by glutathione-sepharose beads coated with BSA (Fraction V) (2 h/4°C) whereas endogenous TAOKs were immunoprecipitated from precleared HaCaT cell lysates using TAOK1 and TAOK2 antibodies (2.5 µg) followed by Protein A agarose beads coated with BSA (Fraction V) (2 h/4°C). All samples were washed three times with lysis buffer and twice with high salt buffer (300 mM NaCl, 12.5 mM

KH_2PO_4/K_2HPO_4 ph7.4). All proteins were eluted in Laemmli sample buffer, resolved by SDS-PAGE and proteins analyzed by immunoblotting.

Immunoblotting

Cells were extracted in lysis buffer and proteins resolved by SDS-PAGE and transferred to 0.2 µm nitrocellulose membranes (GE Healthcare). Membranes were blocked in Tris-buffered saline (TBS) (137 mM NaCl, 20 mM Tris-HCl pH 7.6) containing 5% non-fat dried milk and 0.05% Tween 20 or 3% bovine serum albumin for phospho-specific antibodies. Membranes were incubated with the appropriate primary antibodies in TBS (1 h, room temperature (RT)) followed by HRP-conjugated goat anti-IgG secondary antibodies (1 h, RT) and protein bands visualized using enhanced chemiluminescence (ECL; GE Healthcare) and exposure to film (Fuji) and quantified using densitometry (ImageJ, Fiji).

Immunofluorescence, confocal and time-lapse microscopy

Cells on glass coverslips were fixed with 4% PFA/PBS, permeabilized with 0.2% Triton X-100 in PBS and blocked with 0.2% (w/v) goat serum in PBS for 30 min. Samples were incubated for 1 h with appropriate primary antibodies followed by fluorescein isothiocyanate (FITC)-conjugated goat anti-mouse Alexa-Fluor 488 antibody or anti-rabbit Alexa-Fluor 568 antibody and DAPI (3 µM) to stain DNA. Actin filaments were visualized with 0.1 µg / ml of Alexa Fluor 633-labeled phalloidin (Cy5 conjugated phalloidin) (Merck, Sigma-Aldrich). For Rnd3-pS210 peptide blocking experiments, the Rnd3-pS210 antibody was pretreated for 1 h with 1 µg / ml of either the Rnd3-pS210 phosphorylated peptide or the nonphosphorylated Rnd3-S210 peptide and used to immunostain cells. Coverslips were mounted on Dako mounting medium and images generated using a Zeiss LSM Zen 510 confocal microscope and a 63x / 1.3 NA objective or Nikon A1 inverted confocal microscope with spectral detector and a 60x oil objective. Z-stacks were acquired using a 0.5 µm step size. For live cell time-lapse microscopy, stably transfected mCherry-α-tubulin HeLa cells were plated on 24-well imaging plates (Ibidi) and incubated overnight. For Rnd3 depletion, cells were transfected with the indicated siRNAs and images generated using a spinning disc confocal containing a Ti Microscope with Andor Neo SCC-01950 camera utilizing a Plan Apo VC 20x DIC N2 objective (Nikon). The images were acquired at 15 min intervals over a period of 18 h (73 loops) or 20 h (81 loops) and the experiment completed after 72 h. Images were analyzed using ImageJ (NIH) or NIS Viewer Elements (Nikon) and GraphPad 6.0 software (La Jolla, Ca) where the duration of cytokinesis (intercellular bridge formation to abscission) was determined.

In vitro kinase assays and cell fractionation

For *in vitro* kinase assays, COS-7 cells were electroporated with CMV-FLAG-Rnd3 (wild type (WT) or mutated proteins) or empty CMV-FLAG vector as indicated and after 20 h cell lysates were prepared and FLAG-Rnd3 immunoprecipitated on anti-FLAG agarose beads (2 h/4ºC) (Merck, Sigma-Aldrich). Beads were washed three times, pelleted by centrifugation, and placed in 30 µl kinase buffer (20 mM $MgCl_2$, 2 mM $MnCl_2$, 30 mM Tris-HCl pH 7.4) containing 50 ng purified TAOK1 or TAOK2 (amino acids 1-314) where indicated, 20 µM ATP and 1 µCi [γ-^{32}P]-ATP (Perkin Elmer, 3000Ci / mmol) and incubated for 30 min at 30ºC. Kinase assays were terminated in gel sample buffer and proteins resolved by SDS-PAGE and transferred to nitrocellulose for analysis of protein expression by immunoblotting or detection of labeled proteins by autoradiography and exposure to film (Fuji). For cold kinase assays, [γ-^{32}P]-ATP was replaced by 3 mM ATP and samples incubated for 6 h at 30ºC (Giacomini et al., 2018) and probed with Rnd3-pS210 and GST antibodies. For cell fractionation, electroporated COS-7 cells were harvested in Trypsin-EDTA (Merck, Sigma-Aldrich) and separated into different cell fractions (total, cytosolic, membrane or nucleus) using a cell fractionation kit and according to the manufacturer's instructions (ThermoFisher Scientific). Samples (20 µg) were resolved by SDS-PAGE and proteins present in each fraction detected by immunoblotting with the indicated antibodies.

Statistical analysis

All data were analyzed using GraphPad Prism 6.0 software (La Jolla, Ca). Unless otherwise stated, the data are expressed as the as means ± standard deviation (s.d.), and evaluated using an unpaired two-tailed Mann-Whitney *t*-test for two groups, or by one-way analysis of variance (ANOVA) with Tukey posthoc test for multiple comparisons or two-way ANOVA with Tukey posthoc test or Sidak's test for multiple comparisons. For all analyses, *P*-values ≤ 0.05 were considered statistically significant.

Acknowledgements

We thank Isma Ali, Virginia Castrejon, Monika Gil, Susana Godinho, Costas Mitsopoulos, Roseanna Petrovic, Philippe Riou, Marta Reyes-Corral, Megan Schober and Ignatius Tavares for their helpful advice during the study. We thank Laura Price for a donation to support this work. The study used additional microscopy facilities provided by the Nikon Imaging Center (King's College London).

Competing Interests

The authors declare no competing or financial interests

Author contributions

Conceptualization: R.G., A.R., J.M.; Methodology: R.G., C-Y. K., A.R., J.M.; Validation: R.G., C-Y.K., E.I, C.G; Data curation: R.G., C-Y.K., E.I.; Formal Analysis: R.G., C-Y.K., E.I.; Investigation: R.G., C-Y.K., E.I., C.G., A.R., J.M.; Writing-original draft: R.G., A.R., J.M.; Writing-review and editing: R.G., A.R., J.M.; Visualization: R.G., C-Y.K., E.I., C.G, A.R., J.M.; Supervision: A.R., J.M.; Project administration: A.R., J.M.; Funding acquisition: A.R., J.M.

Funding

This work was supported by Breast Cancer Now (Project Grant 2012NovPR027 to JM), Alzheimer's Research UK (Project Grant IRG2014-6 to JM), Cancer Research UK (Programme Grant CC6620/A15961 to AR) and the King's College Hospital Charity (JM).

REFERENCES

Addi, C., Bai, J. and Echard, A. (2018). Actin, microtubule, septin and ESCRT filament remodeling during late steps of cytokinesis. *Curr Opin Cell Biol* **50**, 27-34.

Aoki, K., Maeda, F., Nagasako, T., Mochizuki, Y., Uchida, S. and Ikenouchi, J. (2016). A RhoA and Rnd3 cycle regulates actin reassembly during membrane blebbing. *Proc Natl Acad Sci U S A* **113**, E1863-71.

Arias-Romero, L. E. and Chernoff, J. (2008). A tale of two Paks. *Biol Cell* **100**, 97-108.

Azzarelli, R., Guillemot, F. and Pacary, E. (2015). Function and regulation of Rnd proteins in cortical projection neuron migration. *Front Neurosci* **9**, 19.

Birkenfeld, J., Nalbant, P., Bohl, B. P., Pertz, O., Hahn, K. M. and Bokoch, G. M. (2007). GEF-H1 modulates localized RhoA activation during cytokinesis under the control of mitotic kinases. *Dev Cell* **12**, 699-712.

Boggiano, J. C., Vanderzalm, P. J. and Fehon, R. G. (2011). Tao-1 phosphorylates Hippo/MST kinases to regulate the Hippo-Salvador-Warts tumor suppressor pathway. *Dev Cell* **21**, 888-95.

Bokoch, G. M. (2003). Biology of the p21-activated kinases. *Annu Rev Biochem* **72**, 743-81.

Chardin, P. (2006). Function and regulation of Rnd proteins. *Nat Rev Mol Cell Biol* **7**, 54-62.

Chen, Z., Hutchison, M. and Cobb, M. H. (1999). Isolation of the protein kinase TAO2 and identification of its mitogen-activated protein kinase/extracellular signal-regulated kinase kinase binding domain. *J Biol Chem* **274**, 28803-7.

Chircop, M. (2014). Rho GTPases as regulators of mitosis and cytokinesis in mammalian cells. *Small GTPases* **5**.

Dan, I., Watanabe, N. M. and Kusumi, A. (2001). The Ste20 group kinases as regulators of MAP kinase cascades. *Trends Cell Biol* **11**, 220-30.

de Anda, F. C., Rosario, A. L., Durak, O., Tran, T., Graff, J., Meletis, K., Rei, D., Soda, T., Madabhushi, R., Ginty, D. D. et al. (2012). Autism spectrum disorder susceptibility gene TAOK2 affects basal dendrite formation in the neocortex. *Nat Neurosci* **15**, 1022-31.

Delpire, E. (2009). The mammalian family of sterile 20p-like protein kinases. *Pflugers Arch* **458**, 953-67.

Derksen, P. W. B. and van de Ven, R. A. H. (2017). Shared mechanisms regulate spatiotemporal RhoA-dependent actomyosin contractility during adhesion and cell division. *Small GTPases*, 1-9.

Estey, M. P., Di Ciano-Oliveira, C., Froese, C. D., Bejide, M. T. and Trimble, W. S. (2010). Distinct roles of septins in cytokinesis: SEPT9 mediates midbody abscission. *J Cell Biol* **191**, 741-9.

Giacomini, C., Koo, C. Y., Yankova, N., Tavares, I. A., Wray, S., Noble, W., Hanger, D. P. and Morris, J. D. H. (2018). A new TAO kinase inhibitor reduces tau phosphorylation at sites associated with neurodegeneration in human tauopathies. *Acta Neuropathol Commun* **6**, 37.

Goh, L. L. and Manser, E. (2012). The GTPase-deficient Rnd proteins are stabilized by their effectors. *J Biol Chem* **287**, 31311-20.

Grill, S. W. and Hyman, A. A. (2005). Spindle positioning by cortical pulling forces. *Dev Cell* **8**, 461-5.

Guasch, R. M., Scambler, P., Jones, G. E. and Ridley, A. J. (1998). RhoE regulates actin cytoskeleton organization and cell migration. *Mol Cell Biol* **18**, 4761-71.

Heng, Y. W. and Koh, C. G. (2010). Actin cytoskeleton dynamics and the cell division cycle. *Int J Biochem Cell Biol* **42**, 1622-33.

Hidalgo-Carcedo, C., Hooper, S., Chaudhry, S. I., Williamson, P., Harrington, K., Leitinger, B. and Sahai, E. (2011). Collective cell migration requires suppression of actomyosin at cell-cell contacts mediated by DDR1 and the cell polarity regulators Par3 and Par6. *Nat Cell Biol* **13**, 49-58.

Hodge, R. G. and Ridley, A. J. (2016). Regulating Rho GTPases and their regulators. *Nat Rev Mol Cell Biol* **17**, 496-510.

Hutchison, M., Berman, K. S. and Cobb, M. H. (1998). Isolation of TAO1, a protein kinase that activates MEKs in stress-activated protein kinase cascades. *J Biol Chem* **273**, 28625-32.

Jaffe, A. B. and Hall, A. (2005). Rho GTPases: biochemistry and biology. *Annu Rev Cell Dev Biol* **21**, 247-69.

Komander, D., Garg, R., Wan, P. T., Ridley, A. J. and Barford, D. (2008). Mechanism of multi-site phosphorylation from a ROCK-I:RhoE complex structure. *EMBO J* **27**, 3175-85.

Koo, C. Y., Giacomini, C., Reyes-Corral, M., Olmos, Y., Tavares, I. A., Marson, C. M., Linardopoulos, S., Tutt, A. N. and Morris, J. D. H. (2017). Targeting TAO Kinases Using a New Inhibitor Compound Delays Mitosis and Induces Mitotic Cell Death in Centrosome Amplified Breast Cancer Cells. *Mol Cancer Ther* **16**, 2410-2421.

Kunda, P. and Baum, B. (2009). The actin cytoskeleton in spindle assembly and positioning. *Trends Cell Biol* **19**, 174-9.

Lancaster, O. M. and Baum, B. (2014). Shaping up to divide: coordinating actin and microtubule cytoskeletal remodelling during mitosis. *Semin Cell Dev Biol* **34**, 109-15.

Liu, T., Rohn, J. L., Picone, R., Kunda, P. and Baum, B. (2010). Tao-1 is a negative regulator of microtubule plus-end growth. *J Cell Sci* **123**, 2708-16.

Maddox, A. S. and Burridge, K. (2003). RhoA is required for cortical retraction and rigidity during mitotic cell rounding. *J Cell Biol* **160**, 255-65.

Madigan, J. P., Bodemann, B. O., Brady, D. C., Dewar, B. J., Keller, P. J., Leitges, M., Philips, M. R., Ridley, A. J., Der, C. J. and Cox, A. D. (2009). Regulation of Rnd3 localization and function by protein kinase C alpha-mediated phosphorylation. *Biochem J* **424**, 153-61.

Manchinelly, S. A., Miller, J. A., Su, L., Miyake, T., Palmer, L., Mikawa, M. and Parsons, S. J. (2010). Mitotic down-regulation of p190RhoGAP is required for the successful completion of cytokinesis. *J Biol Chem* **285**, 26923-32.

Manolaridis, I., Kulkarni, K., Dodd, R. B., Ogasawara, S., Zhang, Z., Bineva, G., Reilly, N. O., Hanrahan, S. J., Thompson, A. J., Cronin, N. et al. (2013). Mechanism of farnesylated CAAX protein processing by the intramembrane protease Rce1. *Nature* **504**, 301-5.

Manukyan, A., Ludwig, K., Sanchez-Manchinelly, S., Parsons, S. J. and Stukenberg, P. T. (2015). A complex of p190RhoGAP-A and anillin modulates RhoA-GTP and the cytokinetic furrow in human cells. *J Cell Sci* **128**, 50-60.

McColl, B., Garg, R., Riou, P., Riento, K. and Ridley, A. J. (2016). Rnd3-induced cell rounding requires interaction with Plexin-B2. *J Cell Sci* **129**, 4046-4056.

Michaelson, D., Silletti, J., Murphy, G., D'Eustachio, P., Rush, M. and Philips, M. R. (2001). Differential localization of Rho GTPases in live cells: regulation by hypervariable regions and RhoGDI binding. *J Cell Biol* **152**, 111-26.

Mitsopoulos, C., Zihni, C., Garg, R., Ridley, A. J. and Morris, J. D. (2003). The prostate-derived sterile 20-like kinase (PSK) regulates microtubule organization and stability. *J Biol Chem* **278**, 18085-91.

Moore, T. M., Garg, R., Johnson, C., Coptcoat, M. J., Ridley, A. J. and Morris, J. D. (2000). PSK, a novel STE20-like kinase derived from prostatic carcinoma that activates the c-Jun N-terminal kinase mitogen-activated protein kinase pathway and regulates actin cytoskeletal organization. *J Biol Chem* **275**, 4311-22.

Nobes, C. D., Lauritzen, I., Mattei, M. G., Paris, S., Hall, A. and Chardin, P. (1998). A new member of the Rho family, Rnd1, promotes disassembly of actin filament structures and loss of cell adhesion. *J Cell Biol* **141**, 187-97.

Pearson, C. G. and Bloom, K. (2004). Dynamic microtubules lead the way for spindle positioning. *Nat Rev Mol Cell Biol* **5**, 481-92.

Piekny, A., Werner, M. and Glotzer, M. (2005). Cytokinesis: welcome to the Rho zone. *Trends Cell Biol* **15**, 651-8.

Piekny, A. J. and Glotzer, M. (2008). Anillin is a scaffold protein that links RhoA, actin, and myosin during cytokinesis. *Curr Biol* **18**, 30-6.

Poon, C. L., Lin, J. I., Zhang, X. and Harvey, K. F. (2011). The sterile 20-like kinase Tao-1 controls tissue growth by regulating the Salvador-Warts-Hippo pathway. *Dev Cell* **21**, 896-906.

Rhys, A. D., Monteiro, P., Smith, C., Vaghela, M., Arnandis, T., Kato, T., Leitinger, B., Sahai, E., McAinsh, A., Charras, G. et al. (2018). Loss of E-cadherin provides tolerance to centrosome amplification in epithelial cancer cells. *J Cell Biol* **217**, 195-209.

Riento, K., Guasch, R. M., Garg, R., Jin, B. and Ridley, A. J. (2003). RhoE binds to ROCK I and inhibits downstream signaling. *Mol Cell Biol* **23**, 4219-29.

Riento, K., Totty, N., Villalonga, P., Garg, R., Guasch, R. and Ridley, A. J. (2005a). RhoE function is regulated by ROCK I-mediated phosphorylation. *EMBO J* **24**, 1170-80.

Riento, K., Villalonga, P., Garg, R. and Ridley, A. (2005b). Function and regulation of RhoE. *Biochem Soc Trans* **33**, 649-51.

Riou, P., Kjaer, S., Garg, R., Purkiss, A., George, R., Cain, R. J., Bineva, G., Reymond, N., McColl, B., Thompson, A. J. et al. (2013). 14-3-3 proteins interact with a hybrid prenyl-phosphorylation motif to inhibit G proteins. *Cell* **153**, 640-53.

Riou, P., Villalonga, P. and Ridley, A. J. (2010). Rnd proteins: multifunctional regulators of the cytoskeleton and cell cycle progression. *Bioessays* **32**, 986-92.

Rosenblatt, J., Cramer, L. P., Baum, B. and McGee, K. M. (2004). Myosin II-dependent cortical movement is required for centrosome separation and positioning during mitotic spindle assembly. *Cell* **117**, 361-72.

Seabra, M. C. (1998). Membrane association and targeting of prenylated Ras-like GTPases. *Cell Signal* **10**, 167-72.

Su, L., Agati, J. M. and Parsons, S. J. (2003). p190RhoGAP is cell cycle regulated and affects cytokinesis. *J Cell Biol* **163**, 571-82.

Tavares, I. A., Touma, D., Lynham, S., Troakes, C., Schober, M., Causevic, M., Garg, R., Noble, W., Killick, R., Bodi, I. et al. (2013). Prostate-derived sterile 20-like kinases (PSKs/TAOKs) phosphorylate tau protein and are activated in tangle-bearing neurons in Alzheimer disease. *J Biol Chem* **288**, 15418-29.

Thery, M. and Bornens, M. (2006). Cell shape and cell division. *Curr Opin Cell Biol* **18**, 648-57.

Timm, T., Li, X. Y., Biernat, J., Jiao, J., Mandelkow, E., Vandekerckhove, J. and Mandelkow, E. M. (2003). MARKK, a Ste20-like kinase, activates the polarity-inducing kinase MARK/PAR-1. *EMBO J* **22**, 5090-101.

Ultanir, S. K., Yadav, S., Hertz, N. T., Oses-Prieto, J. A., Claxton, S., Burlingame, A. L., Shokat, K. M., Jan, L. Y. and Jan, Y. N. (2014). MST3 kinase phosphorylates TAO1/2 to enable Myosin Va function in promoting spine synapse development. *Neuron* **84**, 968-82.

Villalonga, P., Guasch, R. M., Riento, K. and Ridley, A. J. (2004). RhoE inhibits cell cycle progression and Ras-induced transformation. *Mol Cell Biol* **24**, 7829-40.

Wennerberg, K., Forget, M. A., Ellerbroek, S. M., Arthur, W. T., Burridge, K., Settleman, J., Der, C. J. and Hansen, S. H. (2003). Rnd proteins function as RhoA antagonists by activating p190 RhoGAP. *Curr Biol* **13**, 1106-15.

Wojtala, R. L., Tavares, I. A., Morton, P. E., Valderrama, F., Thomas, N. S. and Morris, J. D. (2011). Prostate-derived sterile 20-like kinases (PSKs/TAOKs) are activated in mitosis and contribute to mitotic cell rounding and spindle positioning. *J Biol Chem* **286**, 30161-70.

Yadav, S., Oses-Prieto, J. A., Peters, C. J., Zhou, J., Pleasure, S. J., Burlingame, A. L., Jan, L. Y. and Jan, Y. N. (2017). TAOK2 Kinase Mediates PSD95 Stability and Dendritic Spine Maturation through Septin7 Phosphorylation. *Neuron* **93**, 379-393.

Zhou, T., Raman, M., Gao, Y., Earnest, S., Chen, Z., Machius, M., Cobb, M. H. and Goldsmith, E. J. (2004). Crystal structure of the TAO2 kinase domain: activation and specificity of a Ste20p MAP3K. *Structure* **12**, 1891-900.

Zihni, C., Mitsopoulos, C., Tavares, I. A., Baum, B., Ridley, A. J. and Morris, J. D. (2007). Prostate-derived sterile 20-like kinase 1-alpha induces apoptosis. JNK- and caspase-dependent nuclear localization is a requirement for membrane blebbing. *J Biol Chem* **282**, 6484-93.

Zihni, C., Mitsopoulos, C., Tavares, I. A., Ridley, A. J. and Morris, J. D. (2006). Prostate-derived sterile 20-like kinase 2 (PSK2) regulates apoptotic morphology via C-Jun N-terminal kinase and Rho kinase-1. *J Biol Chem* **281**, 7317-23.

Figures

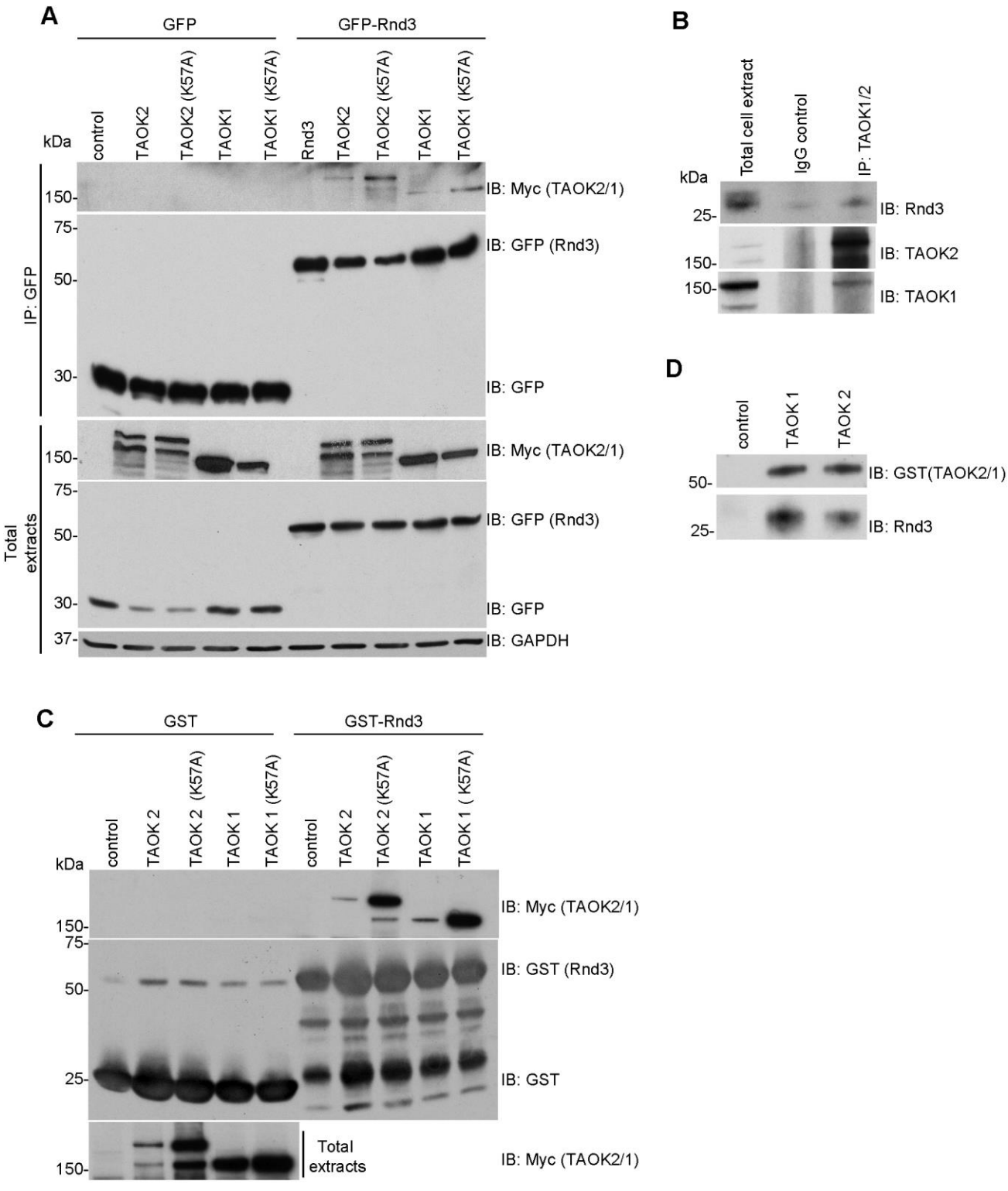

Fig. 1. Rnd3 binds to TAOK1 and TAOK2 in cells and *in vitro*. (A) COS-7 cells were cotransfected with pRK5-Myc empty vector (control), pRK5-Myc-TAOK1, pRK5-Myc-TAOK1 (K57A), pRK5-Myc-TAOK2 or pRK5-Myc-TAOK2 (K57A) and either p-EGFP empty vector or p-EGFP-Rnd3 plasmids as indicated. After 20 h, an aliquot of total extract was taken and lysates incubated with GFP-Trap beads for pulldown assays. Expressed and bound Myc-TAOK proteins were detected by immunoblotting the total extract or bead pellet using anti-Myc antibody. GFP-

Rnd3 or GFP were detected by immunoblotting samples with GFP antibody. Samples were normalized using GAPDH antibody to immunoblot total cell extracts. (B) Cell lysates were prepared from COS-7 cells and aliquots of total extract taken. The remaining samples were divided in two and incubated with IgG (control) or anti-TAOK1/TAOK2 antibody as indicated. Samples were mixed with Protein A agarose and bead pellets probed with antibodies to detect Rnd3, TAOK1 and TAOK2. (C) COS-7 cells were transfected with pRK5-Myc vector (control), pRK5-Myc-TAOK1, pRK5-Myc-TAOK1 (K57A), pRK5-Myc-TAOK2 or pRK5-Myc-TAOK2 (K57A) as indicated. After 20 h, an aliquot of total extract was taken and lysates incubated with GST or GST-Rnd3 immobilized on beads for pulldown assays. Myc-TAOKs in total extracts or bound to GST-Rnd3 were detected by immunoblotting with anti-Myc antibody. GST-Rnd3 and GST were detected using anti-GST antibody. (D) Recombinant His-Rnd3 was incubated in the absence (control) or presence of purified GST-TAOK1 (1-314) or GST-TAOK2 (1-314) as indicated and GST-TAOKs pulled down using glutathione-sepharose beads. Rnd3 and TAOK in the bead pellet were detected by immunoblotting with Rnd3 and GST antibodies respectively. All blots are representative of three independent experiments.

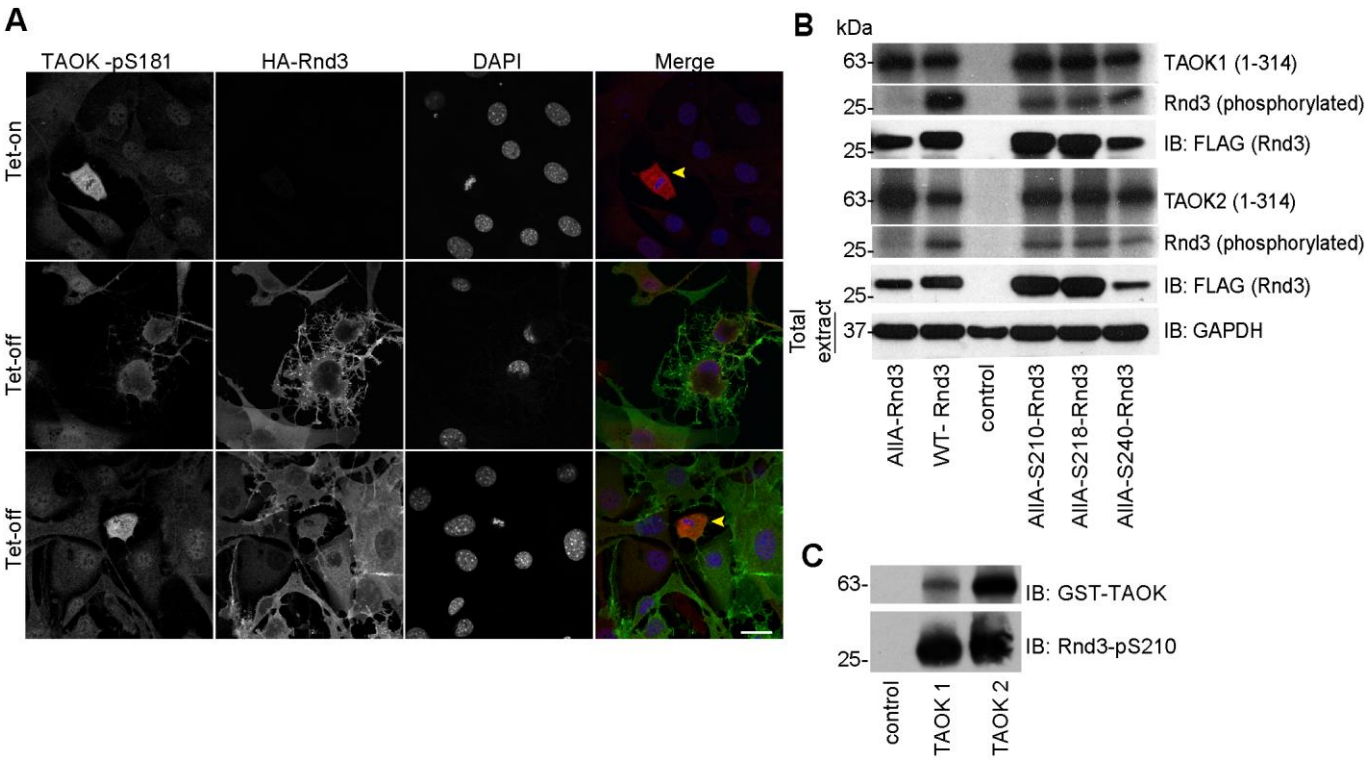

Fig. 2. TAOKs phosphorylate Rnd3 on S210, S218 and S240. (A) NIH3T3-Rnd3 fibroblasts containing a Tet-off inducible HA-Rnd3 construct were incubated in the presence (Tet-on) or absence (Tet-off) of Tet to induce HA-Rnd3 expression. After 8 h, cultures were fixed and stained with antibodies to detect active TAOK-pS181 and HA (HA-Rnd3) plus DAPI (DNA). Arrows point to mitotic cells, which contain active TAOK-pS181 in the presence or absence of Tet and provide a positive TAOK-pS181 antibody control. Scale bar = 10 µm. (B) COS-7 cells were electroporated with CMV-FLAG-Rnd3 (WT), CMV-FLAG-Rnd3 (AllA), CMV-FLAG-Rnd3 (AllA, S210), CMV-FLAG-Rnd3 (AllA, S218), CMV-FLAG-Rnd3 (AllA S240) or CMV-FLAG empty vector (control) as indicated. After 20 h, an aliquot of total extract was taken and lysates incubated with anti-FLAG agarose beads to pulldown FLAG-Rnd3. Samples were mixed with purified GST-TAOK1 (1-314) or GST-TAOK2 (1-314) for *in vitro* kinase assays, resolved by SDS-PAGE and transferred to nitrocellulose for analysis of protein expression by immunoblotting or detection of labeled Rnd3 (~ 27 kDa), TAOK1 or TAOK2 (~ 63 kDa) proteins by autoradiography. Samples were normalized by immunoblotting total extracts with GAPDH antibody. (C) Recombinant His-Rnd3 was incubated in the absence (control) or presence of purified GST-TAOK1 (1-314) or GST-TAOK2 (1-314) for *in vitro* kinase assays and as indicated. Samples were immunoblotted with antibodies to detect Rnd3-pS210 and GST. Images or blots are representative of three independent experiments.

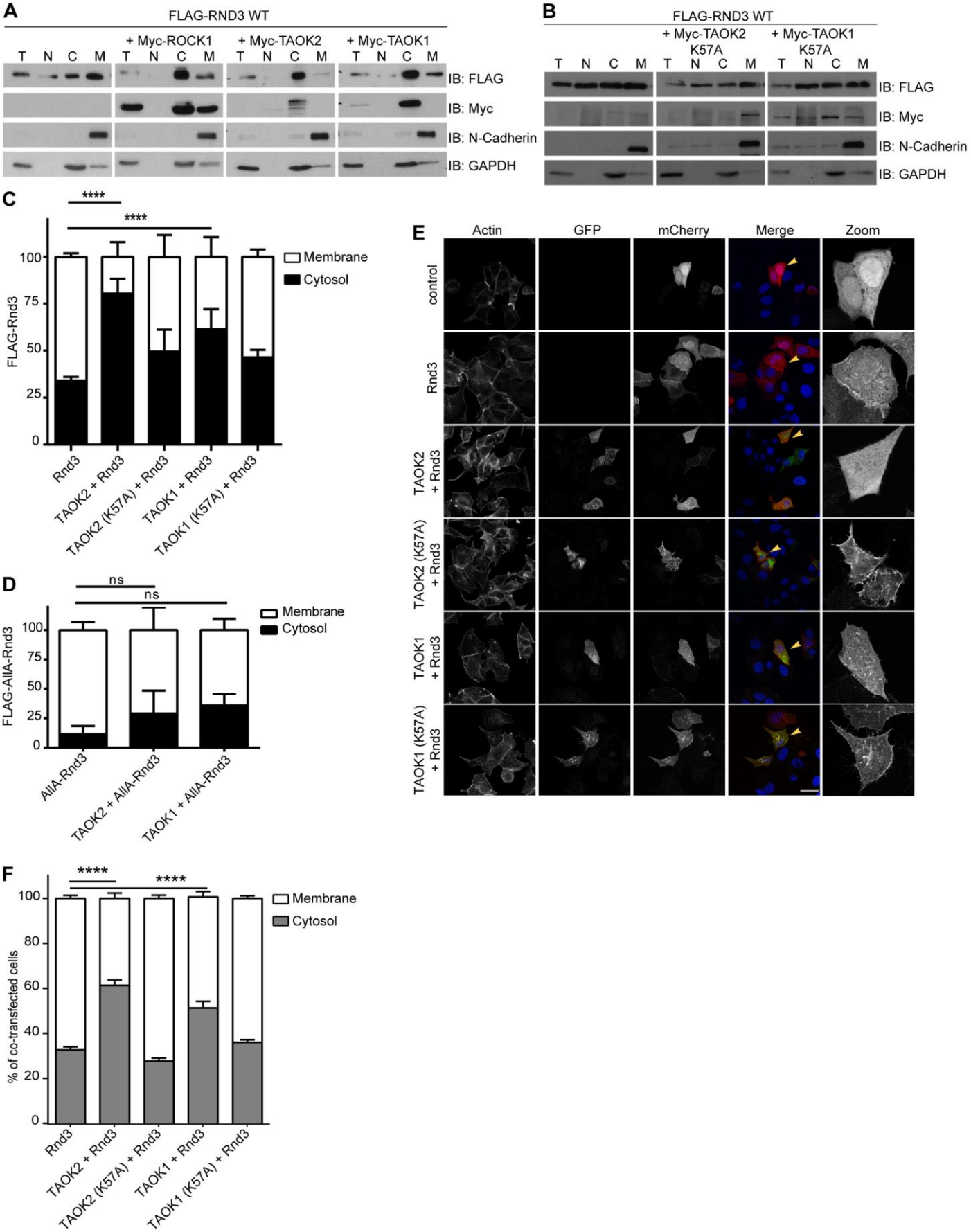

Fig. 3. TAOK1 and TAOK2 relocate Rnd3 from the membrane to the cytosol. COS-7 cells were electroporated with (A) CMV-FLAG-Rnd3 and pRK5-Myc empty vector (control), pRK5-Myc-ROCK1 (1-420), pRK5-Myc-TAOK2 or pRK5-Myc-TAOK1 as indicated or (B) CMV-FLAG-Rnd3 and pRK5-Myc empty vector (control), pRK5-Myc-TAOK1 (K57A) or pRK5-Myc-TAOK2 (K57A) or (D) CMV-FLAG-AIIA-Rnd3 and pRK5-Myc empty vector (control), pRK5-Myc-TAOK1 or pRK5-

Myc-TAOK2 as shown. Cell lysates were prepared after 20 h. An aliquot of total extract (T) was taken and the remaining sample separated into membrane (M), cytosolic (C) or nuclear (N) fractions. All samples were resolved by SDS-PAGE and immunoblotted with antibodies to detect FLAG-Rnd3 (~ 27 kDa), Myc-TAOK1 (~ 150 kDa), Myc-TAOK2 (~ 165 and 175 kDa), Myc-ROCK1 (1-420) (~ 48 kDa), N-Cadherin (~ 140 kDa) or GAPDH (~ 37 kDa). N-Cadherin and GAPDH are markers of membrane and cytosolic fractions, respectively. (C,D) Quantification of the effects of TAOK constructs on FLAG-Rnd3 localization to the membrane or cytosol compared to control cells. Densitometry was used to determine the proportion of Rnd3 in the membrane or cytosol for each experiment and is expressed as a percentage of the total amount in both fractions (100%). Data represent mean±s.d. for three independent experiments. ****P<0.0001 (two-way ANOVA with Tukey posthoc test for multiple comparisons). (E) MCF7 cells were transfected with CB6-GFP-TAOK1, CB6-GFP-TAOK1 (K57A), CB6-GFP-TAOK2 or CB6-GFP-TAOK2 (K57A) and/or mCherry-Rnd3 or mCherry empty vector (control) as indicated and cells fixed after 20 h. Actin filaments were visualized using AlexaFluor 633 conjugated to phalloidin. Arrows point to magnified cells showing localization of mCherry-Rnd3 to the plasma membrane or cytosol. Scale bar = 10 µm. (F) Quantification of the effects of TAOK constructs on mCherry-Rnd3 localization to the membrane or cytosol compared to control cells. > 100 individual cells were selected at random for each condition and per experiment and the presence of mCherry-Rnd3 at the plasma membrane or in the cytosol determined using confocal microscopy. Data represent mean±s.d. of three independent experiments. ****P<0.0001 (two-way ANOVA with Tukey posthoc test for multiple comparisons).

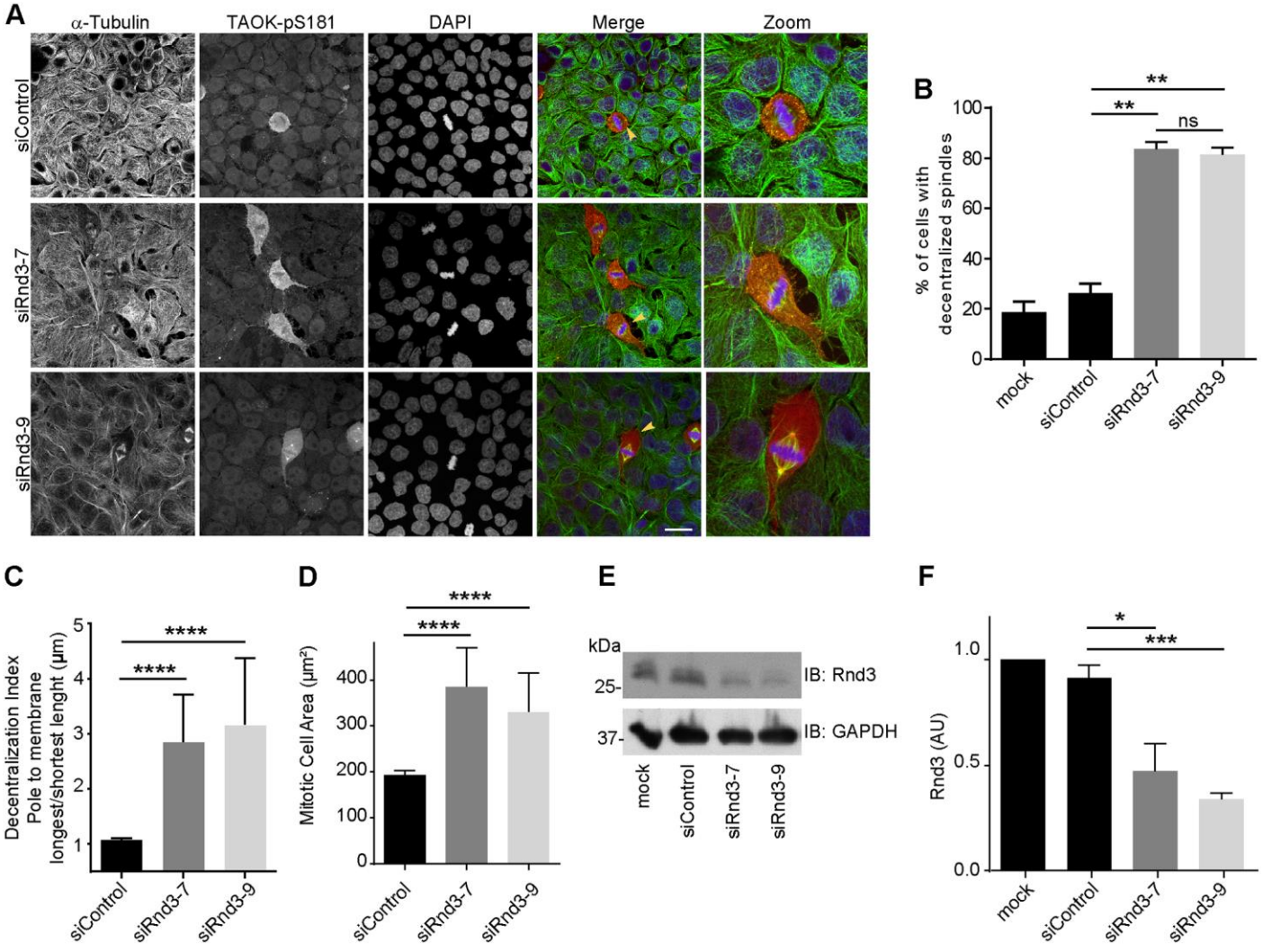

Fig. 4. Rnd3 depletion inhibits mitotic cell rounding and spindle centralization. HeLa cells were transfected with Rnd3 targeting (siRnd3-7, siRnd3-9) or nontargeting (siControl) siRNAs or left untreated (mock) as indicated. After 72 h, cells were fixed and stained with antibodies to detect α-tubulin (microtubules) and active TAOK-pS181 plus DAPI (DNA). (A) Immunofluorescence images showing the effects of Rnd3 depletion on mitotic cell morphology and spindle positioning. Arrows indicate magnified mitotic cells. Scale bar = 10 µm. (B-C) Quantification of spindle decentralization upon Rnd3 depletion. > 30 individual mitotic cells were selected at random for each condition and per experiment and distances between each pole and the closest plasma membrane measured using ImageJ. (B) Graphs show the percentages of mitotic cells with unequal distances and decentralized spindles in siRnd3 depleted cells compared to siControl cells. Data represent mean±s.d. for three individual experiments. $^{**}P<0.01$, ns, not significant (two-tailed Mann-Whitney test). (C) Decentralization index shows the distance between each spindle pole and the closest cell membrane as a ratio of the longest length over the shortest length in siRnd3 depleted cells compared to siControl cells. Data represent mean±s.d. for three independent experiments. $^{****}P<0.0001$ (one-way ANOVA with Tukey posthoc test for multiple comparisons). (D) Graphs show cell spread area for siRnd3 depleted cells compared to siControl

cells. Individual mitotic cells (> 30) were selected at random for each condition and per experiment and the cell periphery encircled and the spread area calculated using ImageJ and GraphPad. Data represent mean±s.d. for three independent experiments. ****P<0.0001 (one-way ANOVA with Tukey posthoc test for multiple comparisons). (E) Residual HeLa cells transfected with the indicated siRNAs (or mock) were lysed and immunoblotted with Rnd3 antibody to confirm Rnd3 depletion and samples normalized using GAPDH antibody. The blot is representative of three independent experiments. (F) Quantification of Rnd3 levels in cells transfected with Rnd3 targeting (siRnd3-7 or siRnd3-9) or nontargeting (siControl) siRNAs. Data represent mean±s.d. for three independent experiments. *P<0.05; ***P<0.001 (one-way ANOVA with Tukey posthoc test for multiple comparisons).

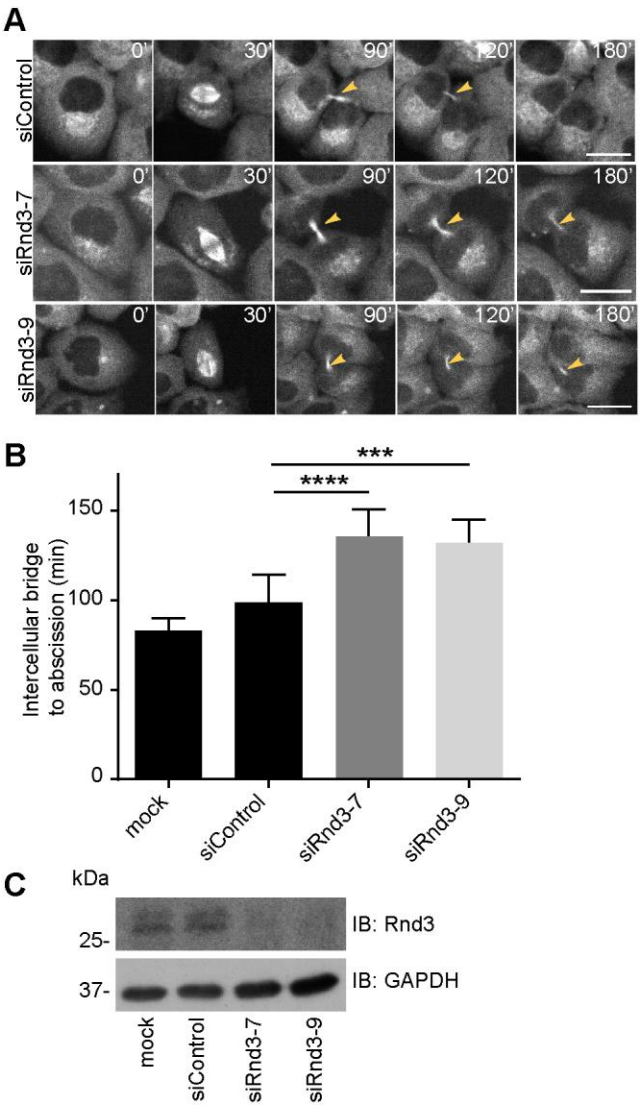

Fig. 5. Rnd3 depletion inhibits cytokinesis. HeLa cells expressing fluorescent mCherry-α–tubulin were untreated (mock) or transfected with Rnd3 targeting (siRnd3-7 or siRnd3-9) or nontargeting (siControl) siRNAs and monitored using time-lapse microscopy. (A) Immunofluorescence images were taken at the indicated time points and show that Rnd3 depletion prolongs cytokinesis. Arrows show breakdown of the intercellular bridge between daughter cells is delayed in the absence of Rnd3. Images are representative of three independent experiments. Scale bar = 10 µm. (B) Quantification of the effect of Rnd3 depletion on cytokinesis. Images were taken at 15 min intervals between 52 h and 72 h post-transfection and individual mitotic cells (> 30 for each condition and per experiment) were selected at random and the time taken (min) between formation of the intercellular bridge and abscission determined using ImageJ (Fiji) and GraphPad. Data represent the mean±s.d. for three independent experiments. ***P<0.001; ****P<0.0001 (one-way ANOVA with Tukey posthoc test for multiple comparisons). (C) A representative blot showing Rnd3 levels. Residual HeLa cells transfected with the indicated siRNAs (or mock) were lysed and immunoblotted with Rnd3 antibody and samples normalized using GAPDH antibody.

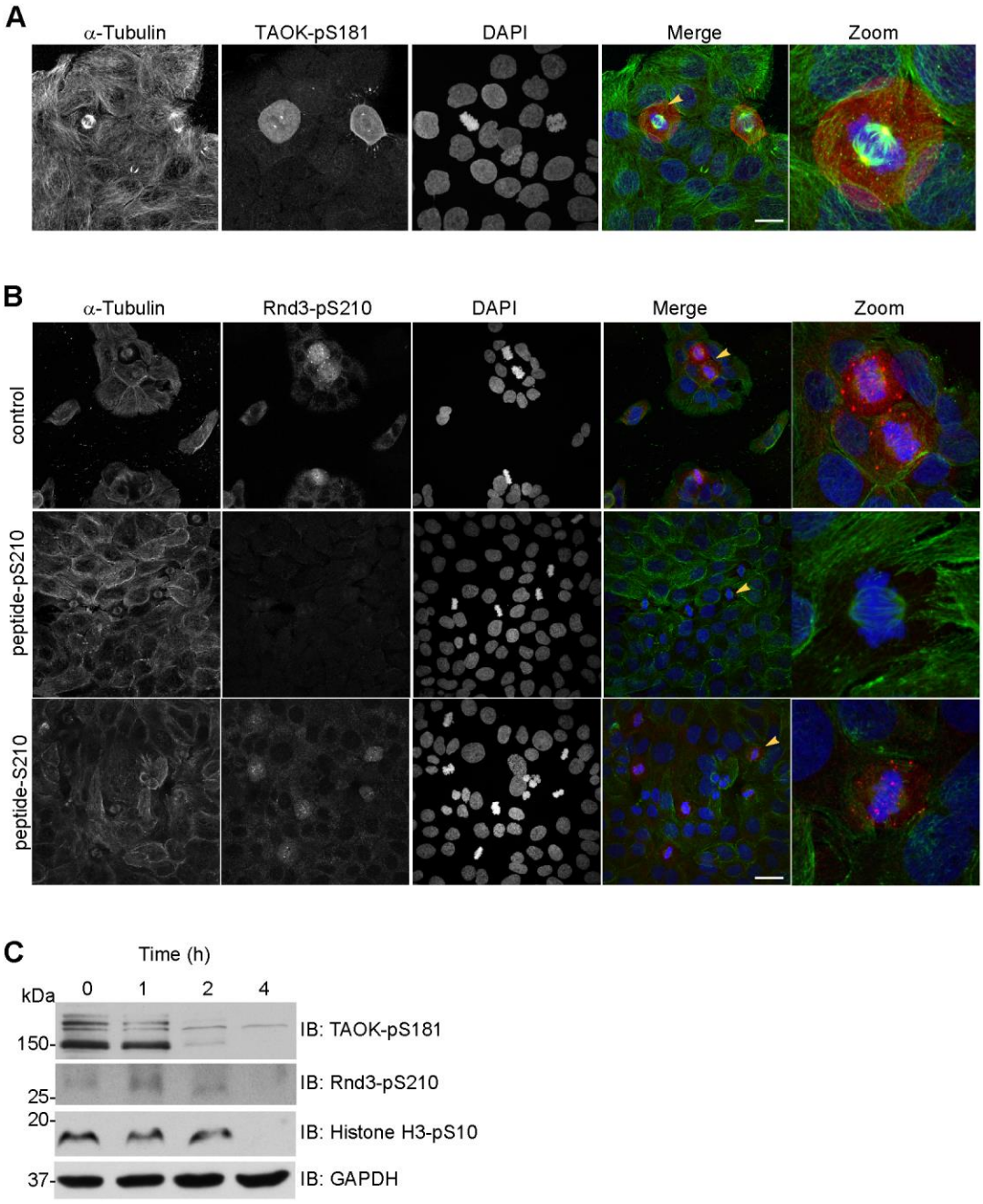

Fig. 6. Active TAOK-pS181 and phosphorylated Rnd3-pS210 are increased in mitotic cells. HaCaT cells were fixed and stained with antibodies to detect (A) α-tubulin (microtubules) and active TAOK-pS181 plus DAPI (DNA) or (B) α–tubulin (microtubules) and Rnd3-pS210 plus DAPI (DNA). For peptide blocking experiments, Rnd3-pS210 antibody was incubated with phosphorylated Rnd3-pS210 or nonphosphorylated Rnd3-S210 peptide (1 µg/ml, 1 h) as indicated before immunostaining fixed cells. Arrows point to magnified mitotic cells. Scale bar = 10 µm. Scale bars = 10 µm. Images are representative of three independent experiments. (C) HaCaT cells were prepared by incubating cultures in excess thymidine (2 mM, 8 h) followed by nocodazole (500 nM) for 12 h. Nocodazole was removed at time zero and cell lysates prepared at the times indicated. Samples were immunoblotted with antibodies to detect active TAOK-pS181, Rnd3-pS210, Histone H3-pS10 (marker for mitosis) and GAPDH. The blot is representative of three independent experiments.

Fig.S1

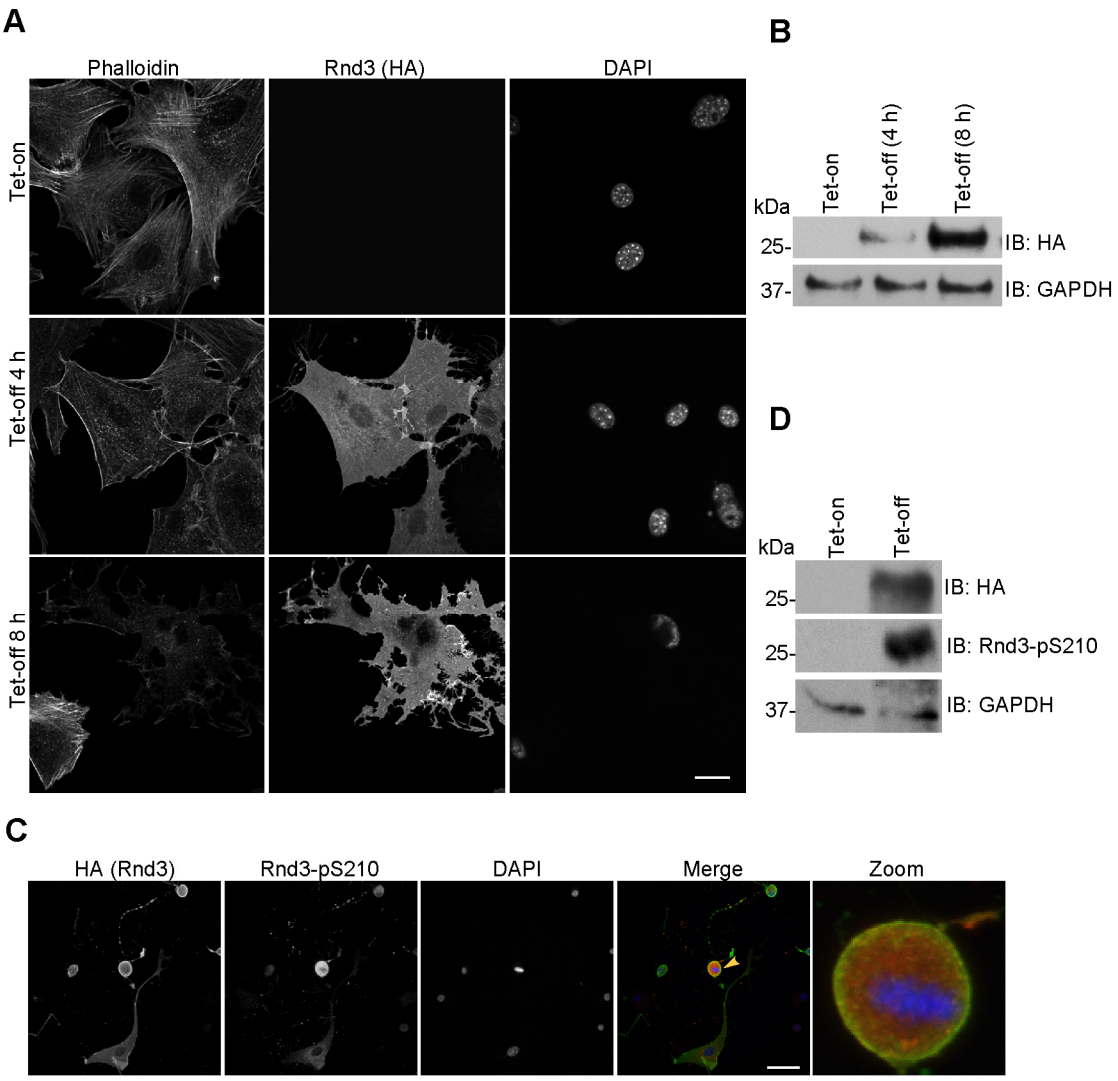

Fig. S1. Induction of Rnd3 expression and Rnd3-pS210 in fibroblasts. NIH3T3-Rnd3 fibroblasts containing a Tet-off inducible HA-Rnd3 construct were incubated in the presence (Tet-on) or absence (Tet-off) of Tet for 8 h to induce HA-Rnd3 expression. (A and C) Cultures were fixed and stained with antibodies to detect HA (HA-Rnd3) or Rnd3-pS210 plus Phalloidin (actin) or DAPI (DNA) as indicated. The arrow indicates a magnified mitotic cell. (C). Images are representative of three independent experiments. Scale bar = 10 µm. (B, D) Cells were lysed and samples immunoblotted with antibodies to detect HA (HA-Rnd3), Rnd3-pS210 and GAPDH as indicated. Blots are representative of three independent experiments.

Fig. S2

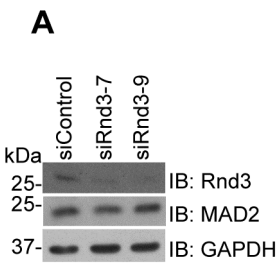

Fig. S2. siRNA depletion of Rnd3. HeLa cells were transfected with Rnd3 targeting (siRnd3-7 or siRnd3-9) or nontargeting (siControl) siRNAs as indicated. After 72 h, cell lysates were prepared and immunoblotted with antibodies to detect Rnd3 or MAD2 and samples were normalized using GAPDH antibody. The blot is representative of two independent experiments.

Fig. S3

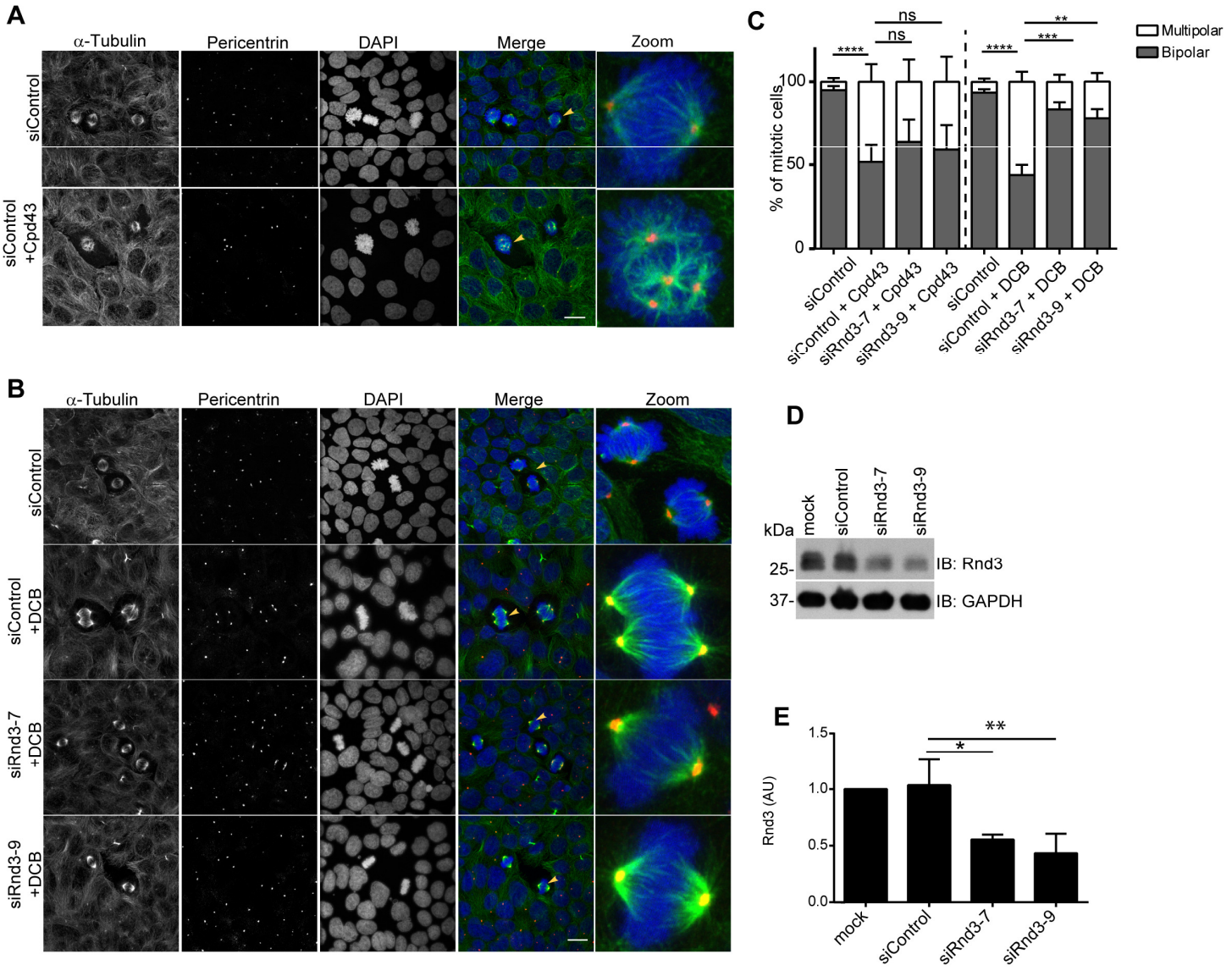

Fig. S3. Rnd3 and TAOKs have opposing effects on spindle multipolarity. HaCaT cells were transfected with Rnd3 targeting (siRnd3-7, siRnd3-9) or nontargeting (siControl) siRNAs as indicated. Cells were (A) incubated with or without TAOK inhibitor Cpd 43 (10 μM) between 48-72 h post transfection and then fixed or (B) incubated with or without DCB (4 μM) between 0-20 h post transfection and then grown in normal medium for a further 24 h and fixed. All samples were stained for α–tubulin (microtubules) and pericentrin (centrosomes) plus DAPI (DNA). Arrows point to magnified mitotic cells displaying bipolar or multipolar spindles. Images are representative of three independent experiments. Scale bar = 20 μm. (C) Quantification of mitotic spindle polarity in siControl cells compared to Cpd43 or DCB treated cells; and DCB treated siControl cells compared to DCB treated Rnd3 depleted cells. > 50 individual mitotic cells were selected at random for each condition and per experiment and the number of spindle poles per cell

established using confocal microscopy. Graphs show an increase in the percentages of mitotic cells displaying multipolar spindles following Cpd43 (left side) or DCB (right side) treatment and that the effect of DCB on spindle multipolarity can be reversed in the absence of Rnd3. Data represents the mean±s.d. for three (DCB) or four (Cpd43) independent experiments. ***P*<0.01, ****P*<0.001, *****P*<0.0001, ns, not significant (two-way ANOVA followed by Sidak's multiple comparison test). (D) Residual HeLa cells transfected with the indicated siRNAs (or mock) were lysed and immunoblotted with Rnd3 antibody to confirm Rnd3 depletion and samples normalized using GAPDH antibody. The blot is representative of three independent experiments. (E) Quantification of Rnd3 levels in cells transfected with Rnd3 targeting (siRnd3-7 or siRnd3-9) or nontargeting (siControl) siRNAs. Data represent mean±s.d. for three independent experiments. **P*<0.05; ***P*<0.01, ns, not significant (one-way ANOVA with Tukey posthoc test for multiple comparisons).

MOVIES

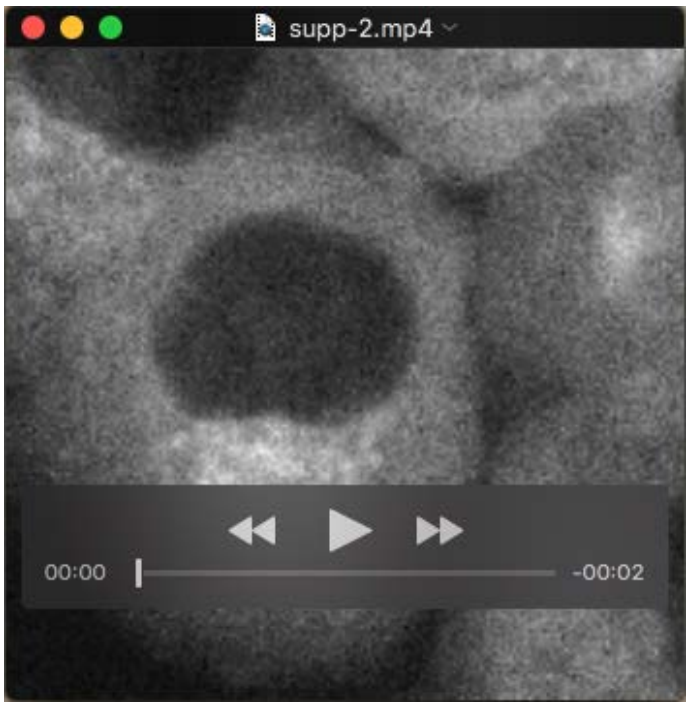

Movie 1. Live images of growing HeLa cells expressing fluorescent mCherry-α–tubulin and transfected with nontargeting (siControl) siRNAs and monitored using time-lapse microscopy.

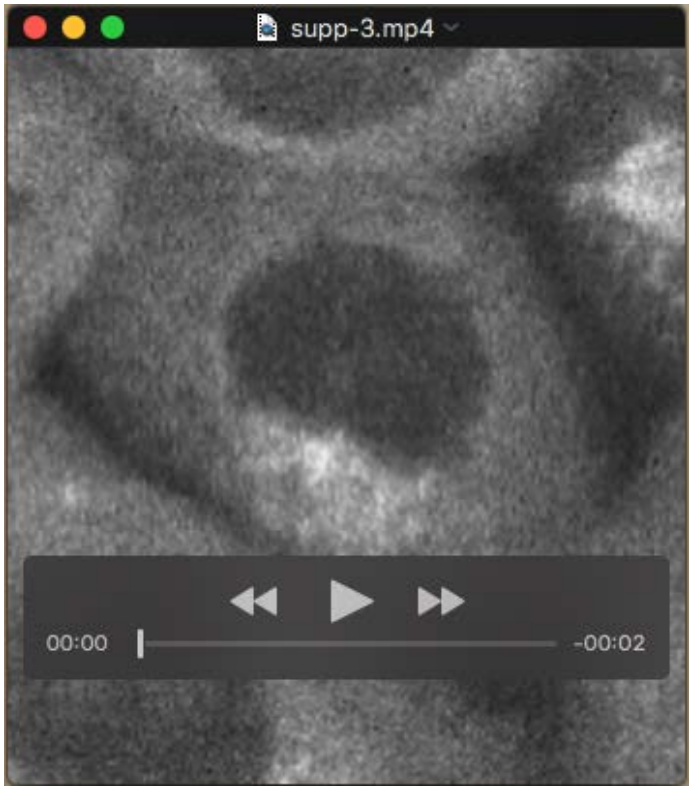

Movie 2. Live images of growing HeLa cells expressing fluorescent mCherry-α–tubulin and transfected with Rnd3 targeting siRNAs (siRnd3-7) and monitored using time-lapse microscopy.

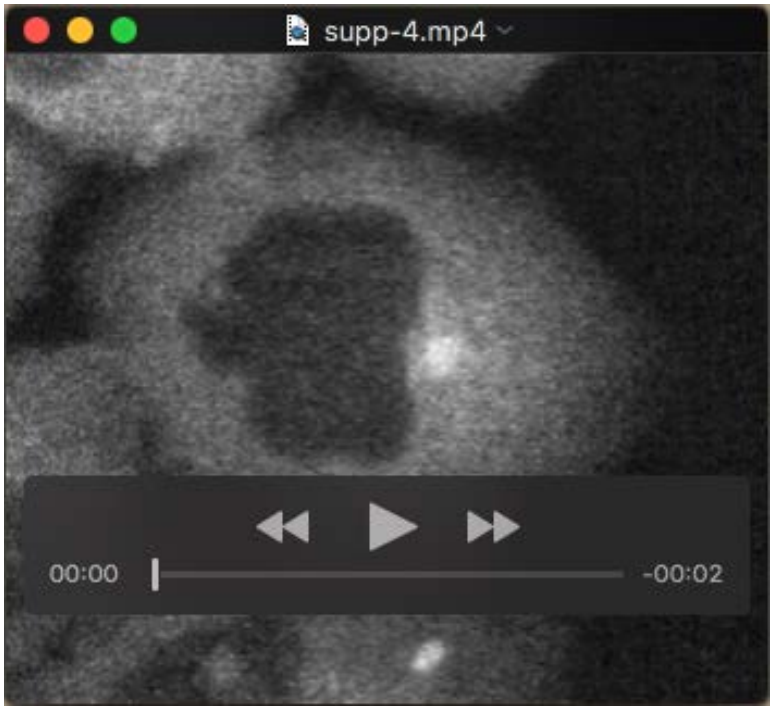

Movie 3. Live images of growing HeLa cells expressing fluorescent mCherry-α–tubulin and transfected with Rnd3 targeting siRNA (siRnd3-9) and monitored using time-lapse microscopy.